1-1-2013

# Enhanced through-the-wall radar imaging using bayesian compressive sensing

V H. Tang
*University of Wollongong*, vht986@uowmail.edu.au

A Bouzerdoum
*University of Wollongong*, bouzer@uow.edu.au

S L. Phung
*University of Wollongong*, phung@uow.edu.au

F H. C Tivive
*University of Wollongong*, tivive@uow.edu.au

# Enhanced through-the-wall radar imaging using bayesian compressive sensing


## Abstract

In this paper, a distributed compressive sensing (CS) model is proposed to recover missing data samples along the temporal frequency domain for through-the-wall radar imaging (TWRI). Existing CS-based approaches recover the signal from each antenna independently, without considering the correlations among measurements. The proposed approach, on the other hand, exploits the structure or correlation in the signals received across the array aperture by using a hierarchical Bayesian model to learn a shared prior for the joint reconstruction of the high-resolution radar profiles. A backprojection method is then applied to form the radar image. Experimental results on real TWRI data show that the proposed approach produces better radar images using fewer measurements compared to existing CS-based TWRI methods. (2013) COPYRIGHT Society of Photo-Optical Instrumentation Engineers (SPIE). Downloading of the abstract is permitted for personal use only.



## Keywords

sensing, imaging, bayesian, radar, wall, enhanced, compressive


## Disciplines

Engineering | Science and Technology Studies


## Publication Details

V. H. Tang, A. Bouzerdoum, S. L. Phung & F. H. C. Tivive, "Enhanced through-the-wall radar imaging using bayesian compressive sensing," in Proceedings of SPIE - Compressive Sensing II, 2013, pp. 87170I-1-87170I-12.

# Enhanced through-the-wall radar imaging using Bayesian compressive sensing

V. H. Tang, A. Bouzerdoum, S. L. Phung and F. H. C. Tivive

School of Electrical, Computer and Telecommunications Engineering,
University of Wollongong, NSW, 2522, Australia

## ABSTRACT

In this paper, a distributed compressive sensing (CS) model is proposed to recover missing data samples along the temporal frequency domain for through-the-wall radar imaging (TWRI). Existing CS-based approaches recover the signal from each antenna independently, without considering the correlations among measurements. The proposed approach, on the other hand, exploits the structure or correlation in the signals received across the array aperture by using a hierarchical Bayesian model to learn a shared prior for the joint reconstruction of the high-resolution radar profiles. A backprojection method is then applied to form the radar image. Experimental results on real TWRI data show that the proposed approach produces better radar images using fewer measurements compared to existing CS-based TWRI methods.

**Keywords:** Through-the-wall radar imaging, delay-and-sum beamforming, compressive sensing, Bayesian compressive sensing, hierarchical Bayesian modeling.

## 1. INTRODUCTION

Through-the-wall radar imaging is an emerging technology that has attracted considerable research interest due to its high demand in numerous civilian and military applications. By transceiving an electromagnetic wave at several locations along an antenna array, TWRI systems provide situational awareness in surveillance operations. For example, a reliable TWRI surveillance system can be used to locate survivors within collapsed buildings in search and rescue missions. Although several imaging approaches have been proposed in the literature,[1–4] there are numerous challenges hindering the development of successful TWRI systems. One of the major impairments of TWRI is that TWRI systems use wideband signals and large aperture arrays for delivering high-resolution imaging in both range and crossrange. This results in prolonged data collection, large storage and high computation cost since a large number of data samples need to be acquired and processed. Moreover, a successful TWRI system should be reliable, portable, and cost-effective. New approaches for TWRI are therefore needed to obtain high-quality images from fewer data samples at a faster speed. To this end, this paper proposes a new approach for TWRI using Bayesian CS. In particular, a distributed CS model along the antenna locations is formulated and a joint Bayesian CS framework is employed to simultaneously reconstruct the range profiles. Once the signals have been recovered, a backprojection method is then adopted for generating the scene image.

The theory of CS enables the reconstruction of sparse or compressible signals from considerably fewer non-adaptive, linear measurements than what is required by the Nyquist-Shannon theorem.[5,6] So far, the application of CS in TWRI can be divided into two main categories. In the first category, TWR image formation is formulated as an inverse problem and CS is applied to reconstruct the imaged scene directly by using linear programming or greedy reconstruction algorithms.[7–9] In the second category, CS is employed in conjunction with traditional beamforming methods. In other words, CS is applied to restore a full data volume, and the conventional image formation methods, such as delay-and-sum (DS) beamforming, is then used to form the image of the scene.[10–12] By exploiting CS, the latter approach enables us to use conventional beamforming methods to reconstruct high-quality images from reduced data samples. Moreover, adopting a conventional image formation approach produces images suitable for the target detection and classification tasks, which typically follow the imaging formation step. Note that a limitation of the traditional beamforming methods is that they require the

Email: vht986@uowmail.edu.au, a.bouzerdoum@uow.edu.au, phung@uow.edu.au, tivive@uow.edu.au.

full data volume to form a high-quality image; otherwise, the image quality deteriorates with the reduction in measurements.[11,12]

In[10] and,[11] the missing data samples along the temporal frequency at each antenna location were recovered by exploiting the sparsity of the received signal. However, the range profile at each antenna location was reconstructed separately, one at a time, using a compressive measurement set collected at the corresponding antenna location only. In TWRI sensing operations, because the same scene of interest is often illuminated by an antenna array placed parallel to the wall from a distance, it is expected that the signals received along the antenna locations experience some dependencies, and their sparsity supports exhibit a certain degree of similarity. Thus, the received signals are jointly sparse, and the correlation between signals should be exploited to enhance the entire reconstruction accuracy.

Inspired by these observations, in this paper, we formulate the range profile reconstructions along the antenna locations as a distributed CS model and aim to reconstruct all the range profiles simultaneously. In the proposed approach, each range profile reconstruction constitutes an inverse problem, and the simultaneous inference problem is formulated in a hierarchical Bayesian setting wherein solving each of the inverse problems corresponds to finding the parameters, i.e., the range profile at each antenna location. Our task is to provide a posterior distribution function for the values of the range vector, given the measurement set. The joint Bayesian CS formulation aims to share information among the different channels by imposing a common hierarchical prior over the various inverse problems. Such hierarchical Bayesian modeling can capture the dependencies between signals without imposing a perfect sparse support between signal coefficient vectors.[13,14]

The remainder of the paper is organized as follows. Section 2 introduces the related work, including TWRI using delay-and-sum beamforming technique, and the conventional CS-based approach in TWRI. Section 3 describes the proposed approach based on joint Bayesian CS framework for TWRI problem. Section 4 presents experimental results and analysis. Section 5 gives concluding remarks.

## 2. RELATED WORK

In this section, the conventional DS beamforming technique and the CS-based method for TWRI are briefly described.

### 2.1 TWRI using DS Beamforming

Consider a stepped-frequency TWRI system that uses $M$ antenna locations and $N$ narrowband signals to image a scene containing $R$ targets. The signal received at the $m$-th antenna location and the $n$-th frequency, $f_n$, is given by

$$z_{m,n} = \sum_{r=0}^{R-1} \sigma_r \, \exp\left\{-j2\pi \, f_n \, \tau_{m,r}\right\}, \tag{1}$$

where $\sigma_r$ is the reflection coefficient of the $r$-th target, and $\tau_{m,r}$ is the round-trip traveling time of the signal from the $m$-th antenna location to the $r$-th target location. In the stepped-frequency approach, the frequency bins $f_n$ are uniformly distributed over the entire frequency band.

The target space behind the wall is partitioned into a rectangular grid, with $N_x$ pixels along the crossrange and $N_y$ pixels along the downrange. Using DS beamforming, a complex image is formed by aggregating the measurements $z_{m,n}$.[1] The value of the pixel at location $(x, y)$ is given by

$$I(x,y) = \frac{1}{MN} \sum_{m=0}^{M-1} \sum_{n=0}^{N-1} z_{m,n} \, \exp\{j2\pi \, f_n \, \tau_{m,(x,y)}\}, \tag{2}$$

where $\tau_{m,(x,y)}$ is the focusing delay between the $m$-th transceiver and the target located at the pixel position $(x, y)$. Assuming that the distance of the transceivers to the front wall, the wall thickness and relative permittivity of wall material are known, the focusing delay can be calculated using Snell's law.[1,2] The process described in (2) is performed for all pixels in the scene to form the radar image.

### 2.2 TWRI using CS

Here, we are interested in the reconstruction of the full measurement set, followed by DS beamforming to obtain the image of the scene; therefore, we will not consider the direct CS approach, where the image of the scene is recovered directly from a set of incomplete measurements. Let $\mathbf{u}_m$ be the discrete range profile and $\mathbf{z}_m$ be the received signal at the $m$-th antenna location. Suppose that the range of interest is partitioned into $L$ equally spaced range cells. Then, the relationship between the measurements given in (1) and the target location can be represented by[11]

$$\mathbf{z}_m = \mathbf{\Psi}\, \mathbf{u}_m, \tag{3}$$

where $\mathbf{z}_m$ is an $N$-dimensional column vector, $\mathbf{\Psi}$ is an $N \times L$ matrix, $[\mathbf{\Psi}]_{nl} = \exp\{-j2\pi\, f_n\, \tau_l\}$, and $\mathbf{u}_m$ is an $L$-dimensional column vector:

$$[\mathbf{u}_m]_l = \begin{cases} \sigma_r, & \text{if } \tau_l = \tau_{m,r}, \\ 0, & \text{otherwise.} \end{cases} \tag{4}$$

In (4), $\tau_l$ is the two-way signal traveling time between the antenna location and location of the $l$-th range cell. Since in indoor imaging the number of targets, or the target area, is very small compared to the whole region of interest, the range vectors $\mathbf{u}_m$ can be considered to be sparse; therefore CS theory can be applied to reconstruct the range profiles from compressive measurements.

Let $\mathbf{y}_m$ be a $K$-dimensional vector consisting of data samples randomly chosen from $\mathbf{z}_m$. The vector $\mathbf{y}_m$ can be expressed as

$$\mathbf{y}_m = \mathbf{\Phi}\, \mathbf{z}_m, \tag{5}$$

where $\mathbf{\Phi}$ is a $K \times N (K < N)$ random selection matrix containing only one non-zero element, which is equal to 1, in each row. From (3), it follows that

$$\mathbf{y}_m = \mathbf{\Phi}\, \mathbf{\Psi}\, \mathbf{u}_m = \widetilde{\mathbf{\Psi}}\, \mathbf{u}_m, \tag{6}$$

where $\widetilde{\mathbf{\Psi}} = \mathbf{\Phi}\, \mathbf{\Psi}$ is a $K \times L$ dictionary matrix. The radar range profiles $\mathbf{u}_m$ can be recovered by solving the following CS inverse problems:

$$\hat{\mathbf{u}}_m = \arg\min_{\mathbf{u}_m} \|\mathbf{u}_m\|_1 \;\text{ subject to }\; \left\| \widetilde{\mathbf{\Psi}}\, \mathbf{u}_m - \mathbf{y}_m \right\|_2 \leq \epsilon, \tag{7}$$

where $\epsilon$ is a noise bound.

In conventional CS, two approaches are usually used to recover the range profiles. In the first approach, the $M$ compressed measurement vectors are concatenated into a single composite measurement vector, which is then used to recover all the range profiles simultaneously; this approach, however, increases the complexity of the problem by $M$-fold. In the second approach, $M$ inverse problems are solved separately to recover $M$ range profiles.[10,11] The conventional CS approach ignores the interdependencies between the signals received across the array aperture. In the next section, we introduce a joint Bayesian CS approach that exploits the signal interdependencies to improve the reconstruction accuracy.

## 3. PROPOSED TWRI APPROACH

In this section, we present the distributed CS model in TWRI, which is formulated based on the joint Bayesian framework for recovering all the range profiles simultaneously. To reduce data acquisition time, CS data collection is performed along the spatial domain, see Fig. 1. Let $\mathbf{y}_m$ denote the compressive measurement sets obtained by randomly selecting a subset of $K_m$ frequencies at the $m$-th antenna location. Mathematically, this CS data acquisition process can be represented using a $K_m \times N$ random selection matrix $\mathbf{\Phi}_m$, which contains zeros, except one entry in each row with value equal to 1. Thus, the reduced measurement vectors $\mathbf{y}_m$ can be expressed as

$$\mathbf{y}_m = \mathbf{\Phi}_m\, \mathbf{z}_m = \mathbf{\Phi}_m\, \mathbf{\Psi}\, \mathbf{u}_m = \mathbf{D}_m\, \mathbf{u}_m, \tag{8}$$

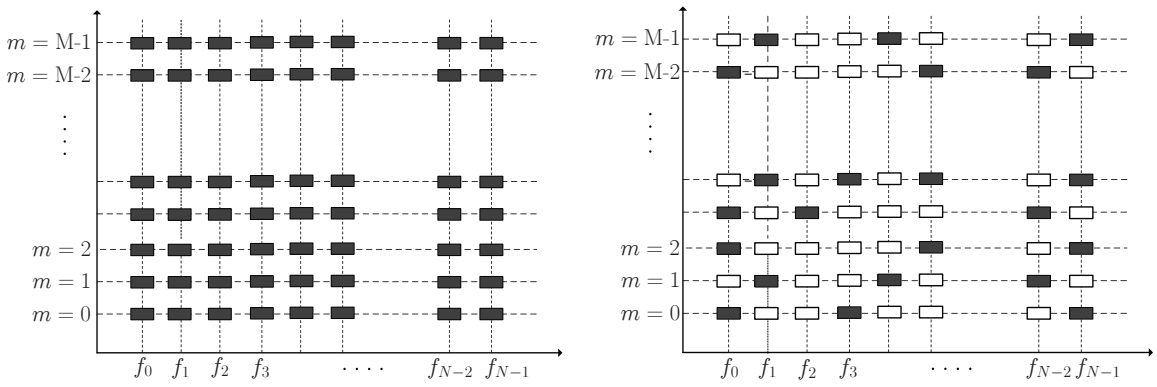


Figure 1. Data acquisition for TWRI: (a) conventional radar imaging scheme; (b) TWRI based on CS. The vertical axis represents the antenna location, and the horizontal axis represents the transmitted frequency. The filled rectangles represent the acquired data samples.

where $\mathbf{D}_m = \mathbf{\Phi}_m \mathbf{\Psi}$, for $m = 0, 1, \ldots, M-1$. To account for noise in the radar signal, the compressive measurement vectors $\mathbf{y}_m$ are modeled as follows:

$$\mathbf{y}_m = \mathbf{D}_m \mathbf{u}_m + \mathbf{v}_m, \tag{9}$$

where $\mathbf{v}_m$ is a vector of additive white Gaussian noise.

Several joint or simultaneous sparse approximation algorithms have been proposed to exploit the structure between signals for improving reconstruction accuracy. Popular joint reconstruction methods include simultaneous orthogonal matching pursuit,[15] multiple-focal underdetermined system solver,[16] and convex relaxation method.[17] However, these approaches suffer from two important shortcomings in TWRI applications. First, they assume that all the signals share a common sparsity support, which does not necessarily hold true in TWRI. In practical TWRI sensing operations, the signals received at several antenna locations experience different attenuation, distortion and multipath effects, causing the signals to have different amplitudes and phases at different receivers. Thus, sparse representation coefficients under a Fourier-like basis, i.e., the range profiles, do not have the same sparsity pattern. Figure 2 depicts the range profiles computed using real radar signals received at several antenna locations. The signals were recorded with a TWR system comprising 57 transceiver locations and 801 step frequencies, illuminating a scene containing a single target. (see Section 4.1 for more information on the radar system setup). Even though the significant nonzero coefficients of the range profiles appear in the vicinity of the target range cell, and thereby resulting in a significant overlap between the support of adjacent range profiles, assuming the same sparsity support for all range profiles may be too restrictive. Second, most methods formulate the problem under the assumption that all of the measurement sets are obtained using the same projection matrix, which in our context corresponds to CS data acquisition using the same frequency bins at all antenna locations. However, having the same frequency observations is not always possible because some individual frequencies or frequency subbands are unavailable due to competing wireless services or intentional interferences.[18] Moreover, because the target reflection coefficients are frequency-dependent, selecting different sets of frequencies for different antennas increases diversity and leads to more information about the target.[19]

To overcome such shortcomings, we propose a new approach based on the joint Bayesian CS to jointly reconstruct all the range profiles by formulating the simultaneous reconstruction problem within a hierarchical Bayesian setting. The graphical Bayesian model assumes that the noise components $\mathbf{v}_m$ are modeled as independent zero-mean Gaussian processes, with precision $\beta$ (variance $1/\beta$):

$$p(\mathbf{v}_m) = \prod_{k=0}^{K_m-1} \mathcal{N}(\mathbf{v}_{m,k}|0, \beta^{-1}). \tag{10}$$

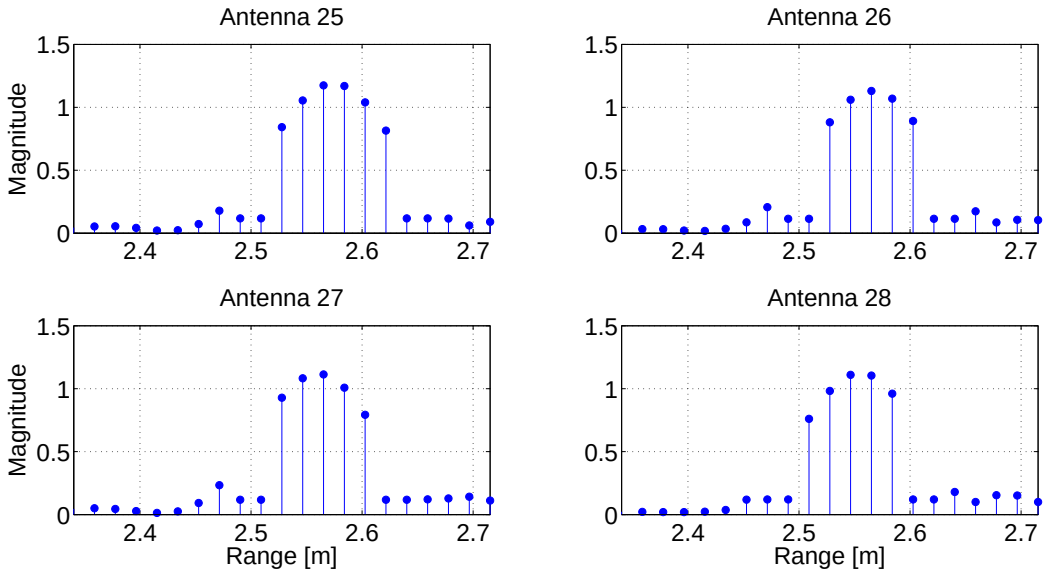


Figure 2. Range profiles computed using full data samples received at several antenna locations in the middle of antenna array.

The noise model therefore implies that the data likelihood function becomes

$$p(\mathbf{y}_m|\mathbf{u}_m,\beta) = (2\pi/\beta)^{-K_m/2}\exp(-\frac{\beta}{2}\,\|\mathbf{y}_m - \mathbf{D}_m\,\mathbf{u}_m\|^2). \tag{11}$$

A hierarchical prior is defined by first assuming that the range profiles $\mathbf{u}_m$ are to be drawn from a product of zero-mean Gaussian distributions with the noise precision determined by the hyperparameters $\boldsymbol{\alpha} = \{\alpha_l\}_{l=0}^{L-1}$,

$$p(\mathbf{u}_m|\boldsymbol{\alpha}) = \prod_{l=0}^{L-1}\mathcal{N}(u_{m,l}|0,\alpha_l^{-1}), \tag{12}$$

and then placing Gamma priors on the hyperparameters $\boldsymbol{\alpha}$ and $\beta$:

$$\begin{aligned} p(\boldsymbol{\alpha}|a,b) &= \prod_{l=0}^{L-1}\Gamma(\alpha_l|a,b), \\ &= \prod_{l=0}^{L-1} b^a\,\alpha_l^{a-1}\,\exp(-b\,\alpha_l)\,\Gamma(a)^{-1}, \qquad (13) \\ p(\beta|c,d) &= \Gamma(\beta|c,d), \qquad (14) \end{aligned}$$

where $\Gamma(\xi)$ is the gamma function:

$$\Gamma(\xi) = \int_0^\infty t^{\xi-1}\,e^{-t}\,dt. \tag{15}$$

To see why the combination of Gaussian and Gamma priors promotes a sparse representation, we consider marginalizing over the vector of hyperparameters $\boldsymbol{\alpha}$. The overall prior on $\mathbf{u}_m$ corresponds to the Student-t distribution which is known to promote sparsity.[13,20] Specifically, with appropriate choice of $a$ and $b$ in (13), the prior favors most $u_{m,l}$ to be zero, i.e., it is a sparseness prior.

The graphical Bayesian representation for TWRI problem is visualized in Fig. 3. In this hierarchical representation, the hyperparameters $\boldsymbol{\alpha} = \{\alpha_l\}_{l=0}^{L-1}$ are shared among all the $M$ inverse tasks. This therefore allows all the compressive measurements $\{\mathbf{y}_m\}_{m=0}^{M-1}$ to contribute to learning the shared hyperparameters, offering the

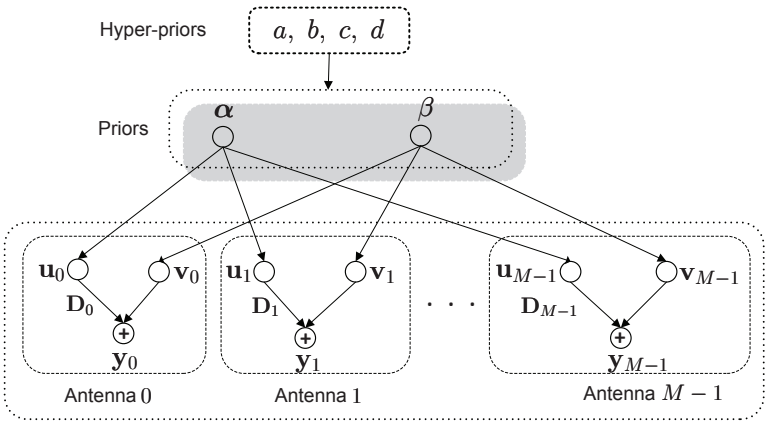


Figure 3. Hierarchical Bayesian model for the joint range profile reconstruction in the TWRI problem.

opportunity to adaptively exploit the dependences between different measurement sets. Note that once the hyperparameters $\boldsymbol{\alpha}$ have been estimated, the range profiles $\mathbf{u}_m$ are learned individually. Thus, the commonality between signals are exploited while the individuality is preserved in this graphical representation. It is important to note that each element of the shared hyperparameters $\boldsymbol{\alpha}$ is used to guarantee the strength of the corresponding component of the range profiles $\mathbf{u}_m$. Specifically, a value $\alpha_l$ diverging to infinity implies that the values $u_{m,l}$ are equal to zero due to the zero-mean and zero-variance Gaussian prior at this location, while a finite $\alpha_l$ does not constrain all $M$ range profile values at the $l$-th location to be nonzero. The hierarchical Bayesian model therefore captures the diversity of sparsity patterns across the range profiles $\mathbf{u}_m$.

Applying the Bayes' rule, from the data likelihood (11) and the hierarchical prior (12), the posterior density function for the range profiles $\mathbf{u}_m$ are given by

$$p(\mathbf{u}_m|\mathbf{y}_m, \boldsymbol{\alpha}, \beta) = \frac{p(\mathbf{y}_m|\mathbf{u}_m, \beta)\, p(\mathbf{u}_m|\boldsymbol{\alpha})}{p(\mathbf{y}_m|\boldsymbol{\alpha}, \beta)}. \tag{16}$$

Because both the data likelihood and the prior are Gaussian functions, the posterior distribution for $\mathbf{u}_m$ can be evaluated analytically, which turns out to be a multivariate Gaussian distribution $\mathcal{N}(\mathbf{u}_m|\boldsymbol{\mu}_m, \Sigma_m)$ with mean and covariance given by,[13,20]

$$\boldsymbol{\mu}_m = \beta\, \Sigma_m\, \mathbf{D}_m^H\, \mathbf{y}_m, \tag{17}$$

$$\Sigma_m = (\beta\, \mathbf{D}_m^H\, \mathbf{D}_m + \mathbf{A})^{-1}, \tag{18}$$

where $\mathbf{A} = \mathrm{diag}(\alpha_0, \alpha_1, \ldots, \alpha_{L-1})$. For a more robust shrinkage and information sharing, the signal prior (12) is modified to integrate out the noise precision $\beta$,[14]

$$p(\mathbf{u}_m|\boldsymbol{\alpha}, \beta) = \prod_{l=0}^{L-1} \mathcal{N}(u_{m,l}|0, \beta^{-1}, \alpha_l^{-1}). \tag{19}$$

This modification changes the posterior of the range profiles $\mathbf{u}_m$ from a multivariate Gaussian distribution to a multivariate Student-t distribution, with the following mean and covariance:[14]

$$\boldsymbol{\mu}_m = \Sigma_m\, \mathbf{D}_m^H\, \mathbf{y}_m, \tag{20}$$

$$\Sigma_m = (\mathbf{D}_m^H\, \mathbf{D}_m + \mathbf{A})^{-1}. \tag{21}$$

So far, we have obtained an expression for the posterior $p(\mathbf{u}_m|\mathbf{y}_m, \boldsymbol{\alpha})$, all we need to do is to find a point estimate for the shared hyperparameters $\boldsymbol{\alpha}$. This is achieved by finding the hyperparameters that maximize the marginal likelihood, or equivalently, its logarithm:

$$\hat{\boldsymbol{\alpha}} = \arg\max_{\boldsymbol{\alpha}} \mathcal{L}(\boldsymbol{\alpha}), \tag{22}$$

where

$$\mathcal{L}(\boldsymbol{\alpha}) = \sum_{m=0}^{M-1} \log p(\mathbf{y}_m|\boldsymbol{\alpha}) = \sum_{m=0}^{M-1} \log \int p(\mathbf{y}_m|\mathbf{u}_m, \beta) p(\mathbf{u}_m|\boldsymbol{\alpha}, \beta) p(\beta, a, b) d\mathbf{u}_m d\beta. \quad (23)$$

Such optimization process is called type-II maximum-likelihood (ML) procedure, which is solved effectively via an iterative estimation[13,20] or a sparse Bayesian approximation.[14] Once the point estimates $\hat{\boldsymbol{\alpha}}$ have been obtained, the approximate range profiles $\widehat{\mathbf{u}}_m$ are given by the mean values of the posterior densities $p(\mathbf{u}_m|\mathbf{y}_m, \boldsymbol{\alpha})$. Here, we emphasize that all the measurements from $M$ antenna locations contribute to the maximization procedure via the summation over the conditional distributions in (23). Hence, the information sharing across the signals occurs through this collaboration in the ML estimation of the hyperparameters. Once the point estimates are constituted using all measurement sets, the posterior for the range profile $\mathbf{u}_m$ is estimated based only on its data set $\mathbf{y}_m$, using mean and variance given in (20).

After all the range profiles $\mathbf{u}_m$ have been obtained, the full data volume $\mathbf{z}$ is recovered using (3); finally, DS beamforming is applied to form the scene image as described in Section 2.1. In the next sections, the performance of the proposed joint Bayesian compressive sensing (JBCS) approach is evaluated on real TWRI data. The imaging results are compared with the conventional DS beamforming and CS-based methods.

## 4. EXPERIMENTAL RESULTS AND ANALYSIS

In this section, the proposed approach is evaluated using real TWRI data sets. The experimental setup for radar signal acquisition along with the imaging results and discussions are presented in the following subsections.

### 4.1 Experimental Setup

The proposed approach was evaluated on real TWR data collected at the Radar Imaging Laboratory of the Center for Advanced Communications, Villanova University, USA. The radar system was placed in front of a concrete wall of thickness 0.143 m, and relative permittivity $\epsilon_r = 7.6$. The imaged scene is depicted in Fig. 4. It contains a 0.4 m high and 0.3 m wide dihedral, placed on a turntable made of two 1.2 m x 2.4 m sheets of 0.013 m thick plywood. A step-frequency signal between 0.7 and 3.1 GHz, with 3 MHz frequency step, was used to illuminate the scene. The antenna array was placed at a height of 1.22 m above the floor and a standoff distance of 1.016 m away from the wall. The antenna array was 1.24 m long, with inter-element spacing of 0.022 m. Therefore, the number of antenna elements and number of frequencies used to image the scene are, respectively, $M = 57$ and $N = 801$, and the total number of measurements is $M \times N$ =45,657 samples. The imaged scene, extending from [0, 4] m in downrange and [−2, 2] m in crossrange, was partitioned into an image of size $65 \times 65$ pixels. Several algorithms have been proposed to solve single CS inverse problems. In this paper, we adopted an $\ell_1$ optimization algorithm called basis pursuit denoising (BPDN)[21] for solving the sparse approximation problems (7) in the conventional CS approach because this algorithm produces stable and accurate solutions and is more robust to noise. The noise bound $\epsilon$ was estimated using a cross-validation strategy.[22]

### 4.2 Performance Measure

To quantify the performance of the various imaging methods, we use the target-to-clutter ratio (TCR) as a measure of quality of reconstructed images.[4] Let $P_r$ denote the average power of region $r$ in the reconstructed image $I$, where $r$ is a target or clutter region. The average power $P_r$ can be expressed as

$$P_r = \frac{1}{N_r} \sum_{(x,y)\in r} I_r^2(x, y), \quad (24)$$

where $N_r$ is the number of pixels in region $r$. The TCR is defined as the ratio between the average power of the target region and the average power of the clutter region (in dBs):

$$\text{TCR} = 20 \log_{10} \left\{ \frac{P_{\text{target}}}{P_{\text{clutter}}} \right\}. \quad (25)$$

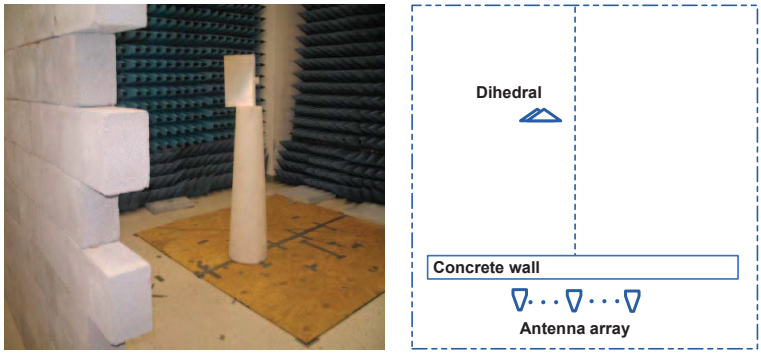


Figure 4. TWRI data acquisition. Left: a photo of the scene; Right: a top-view of the behind-the-wall scene.

The clutter region is the entire reconstructed image, excluding the target region. The target region is a $2 \times 6$ area selected manually in the vicinity of the target.

### 4.3 Results and Analysis

For reference purposes, Fig. 5(a) presents the image formed by the standard DS beamforming method using all the frequency bins (i.e., full data samples). Note that in this paper, all output images are normalized by the maximum image intensity. The true target position is indicated with a solid white rectangle. Using the full data samples, the conventional DS beamforming yields a high-quality image with TCR = 54.23 dB. However, when the number of samples is significantly reduced, the standard DS beamforming method alone does not yield a high-quality image. Figure 5(b) shows the image formed using measurement sets acquired by randomly selecting 24 frequency bins at each antenna location (i.e., 3% of the full data samples). Clearly, this image contains many false targets, and has a TCR = 27.70 dB. Fig. 5(c) shows the image obtained with the conventional CS approach, using the same data set as in Figure 5(b). This is a dramatically degraded image with TCR = 30.08 dB. By comparison, the proposed JBCS approach yields an image with a well localized target and a TCR of 43.38 dB, see Fig. 5(d). Thus, the proposed JBCS approach produces a higher image quality, compared to conventional DS beamforming and CS methods, using the same number of reduced measurements. Figure 6 shows the reconstructed range profiles by the conventional CS and the proposed JBCS approaches. The CS method reconstructs the range profiles where the large values of the range bins spread widely (Fig. 6(a)). In contrast, the proposed JBCS approach produces the range profiles where the significant range values properly represent the dihedral target range cells (Fig. 6(b)).

In the next experiment, the performances of the different imaging approaches are evaluated using compressive measurement sets acquired using 80 frequency bins at each antenna (i.e., 10% of the full data volume). Figure 7(a) presents the reconstructed image with the conventional CS approach. Although the target is detected, clutter and background noise are prominent in the formed image (TCR = 42.58 dB). Figure 7(b) shows the reconstructed image with the proposed JBCS approach. It is evident that this formed image is of significantly higher quality (TCR = 54.72 dB): the true target is accurately located and the clutter is significantly suppressed. Furthermore, the quality of the image reconstructed by the proposed JBCS approach, using just 10% of full data samples, is comparable to that of the image formed with the DS beamforming using full data volume, shown in Fig. 5(a).

The next experiment evaluates the effectiveness of the joint reconstruction of the range profiles with the JBCS approach. The number of frequency bins used was fixed at 10% and the set of antenna locations was varied from 1 to 57. For each subset of measurements, the experiment was repeated 50 times and the average mean square error (MSE) between the original and reconstructed range profiles with the conventional CS and the proposed JBCS approaches were computed. Figure 8 shows the average MSE of the conventional CS and the proposed JBCS-based approaches, as a function of number of antenna locations. It is evident from the figure that joint reconstruction using several measurement sets produces range profiles with much higher reconstruction accuracy than separate reconstruction of the range profiles.

To evaluate the robustness of the proposed approach, several different measurement sets were acquired by varying the number of frequency bins used. For each set of measurements, the experiment was repeated 50

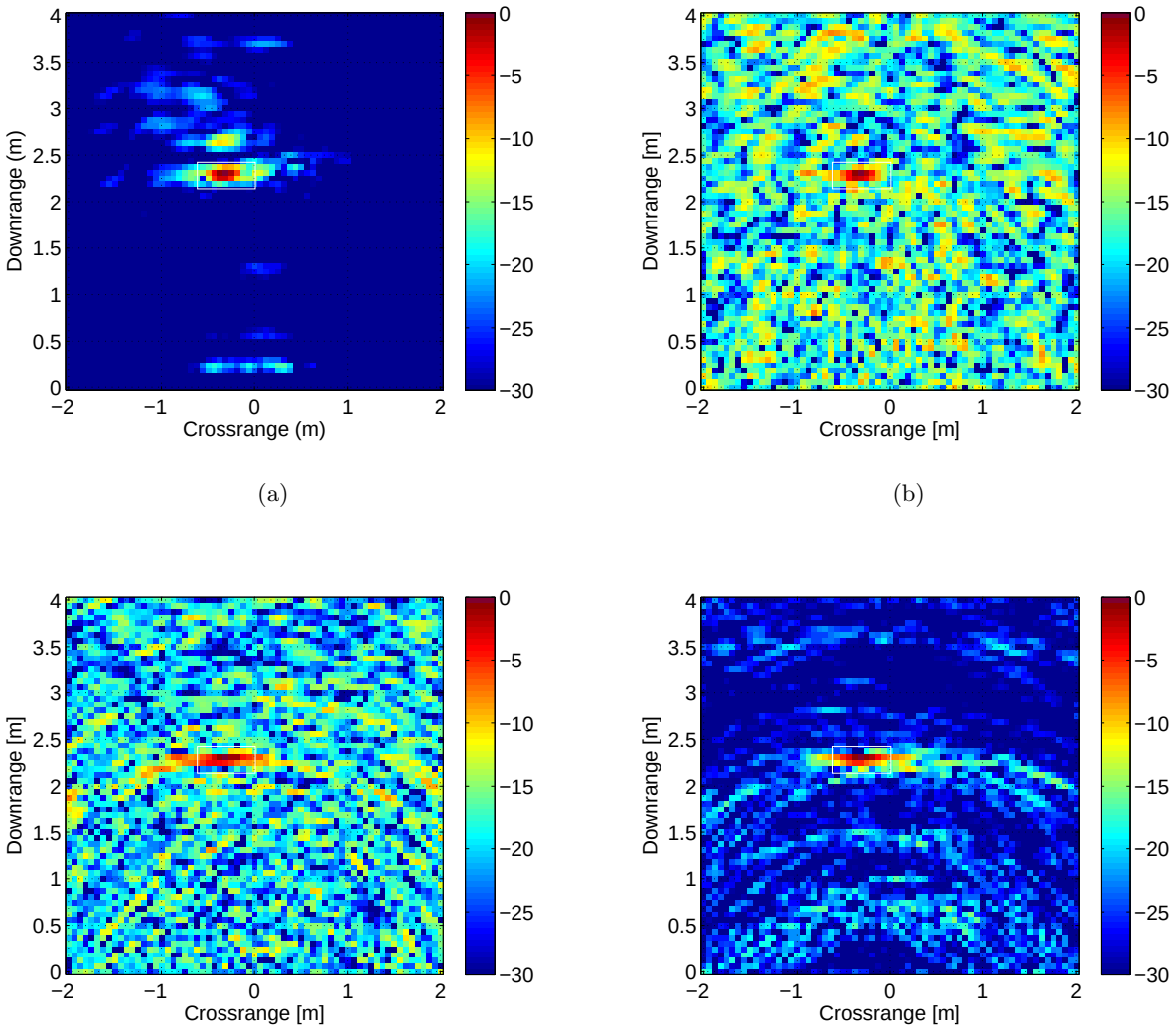


Figure 5. Images produced by different TWRI approaches (a) DS beamforming using full data samples (TCR = 54.23 dB); (b) DS beamforming using 3% of full data samples (TCR = 27.70 dB); (c) CS using 3% of full data samples (TCR = 30.08 dB); (d) proposed JBCS using 3% of full data samples (TCR = 43.38 dB).

times, and the average TCR of the reconstructed images was computed. Figure 9 illustrates average TCR of images reconstructed using the conventional DS beamforming, the CS and the proposed JBCS-based TWRI approaches as a function of the ratio between the reduced and the full measurement set. These results indicate the followings: 1) the proposed JBCS-based TWRI approach outperforms the conventional DS beamforming and CS-based approaches in terms of TCR. For example, using 20% of the full measurements (i.e., 120 frequency bins), DS beamforming, the traditional CS and the proposed JBCS yield images with, respectively, TCR of 40.70 dB, 47.12 dB and 55.10 dB. 2) the proposed approach produces TWRI images with slightly higher TCR (TCR = 57.77 dB), using just 25% frequency bins, compared to the conventional DS beamforming method using full measurement set (TCR = 54.23 dB).

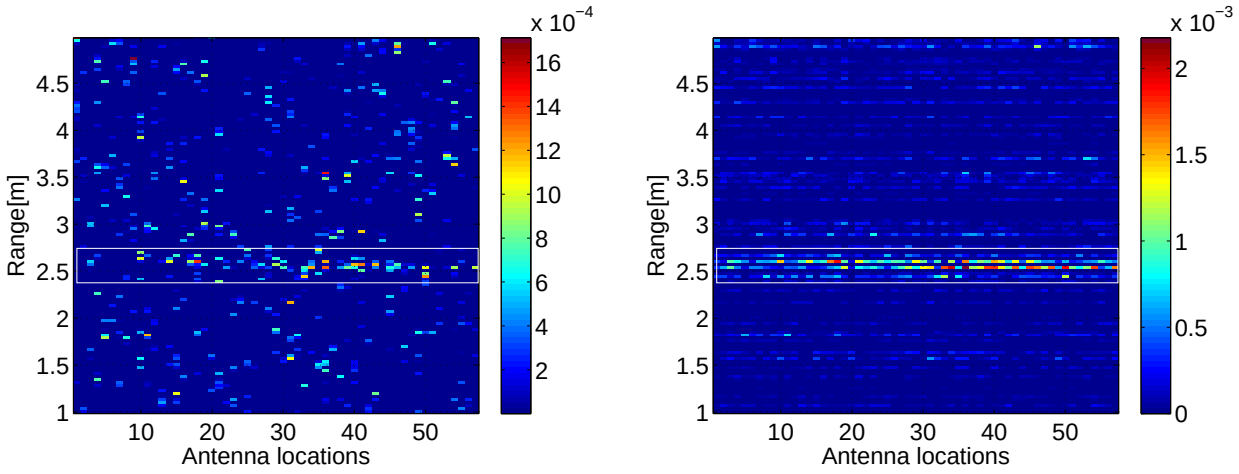


(a) (b)

Figure 6. Comparison of the radar range profiles: (a) reconstructed by the conventional CS approach using 3% of full data samples; (b) reconstructed by the proposed JBCS approach using 3% of full data samples.

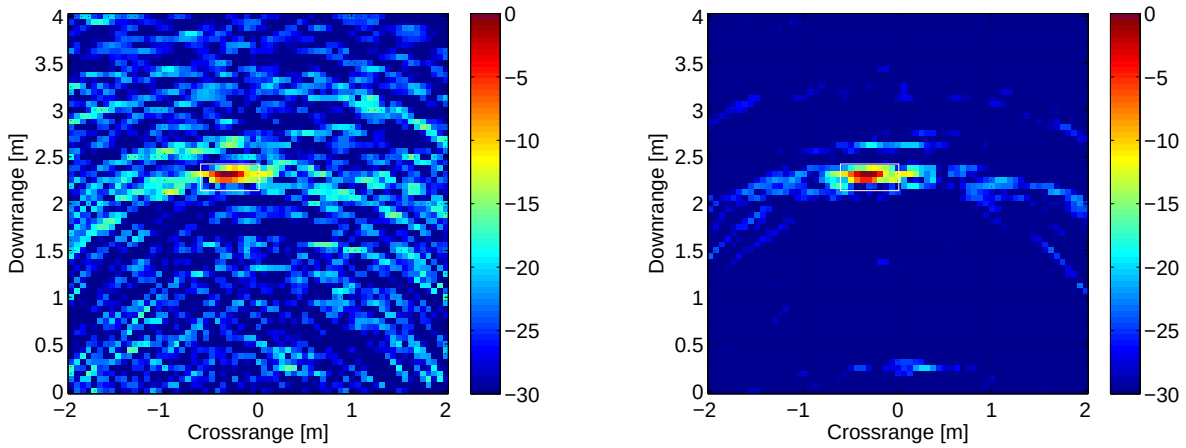


(a) (b)

Figure 7. Images produced by different TWRI approaches: (a) the conventional CS approach (TCR = 42.58 dB); (b) the proposed JBCS approach (TCR = 54.72 dB). Here, 10% of the full data volume were used.

## 5. CONCLUSION

In this paper, we presented a new TWRI approach based on Bayesian compressive sensing. A novel distributed CS model is proposed for TWRI, where the problem is formulated using a hierarchical Bayesian model for joint reconstruction of the range profiles at different antenna locations. The experimental results using real TWRI data demonstrate the effectiveness and robustness of the proposed approach. This is made possible because the joint Bayesian approach promotes the sparsity of each signal, while exploits the correlation between different measurement sets for the joint range profile reconstruction. The commonality between signals is exploited while the individuality is preserved in this graphical Bayesian representation. The new approach produces images where the targets are accurately located and highlighted and the clutter is significantly suppressed. Therefore, it would be reasonable to expect that the proposed approach will enhance TWRI target detection, localization

and classification, while allowing a considerable reduction in the number of measurements and data acquisition time.

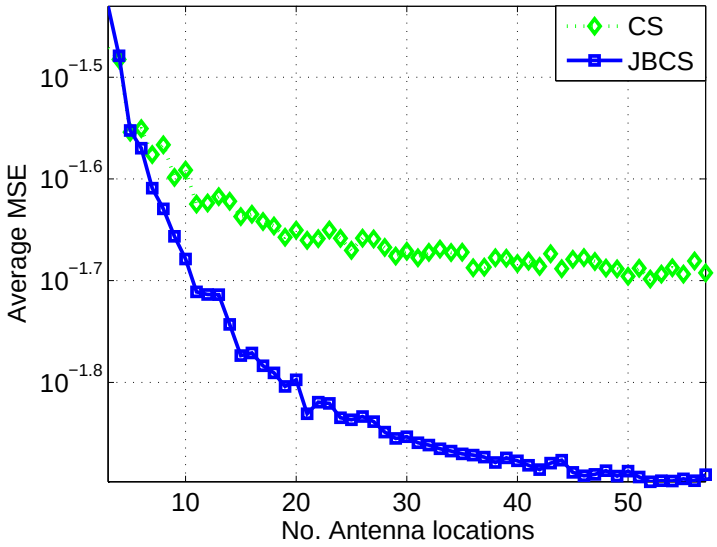


Figure 8. The average MSE of range profiles reconstructed by the conventional CS and the proposed JBCS approaches.

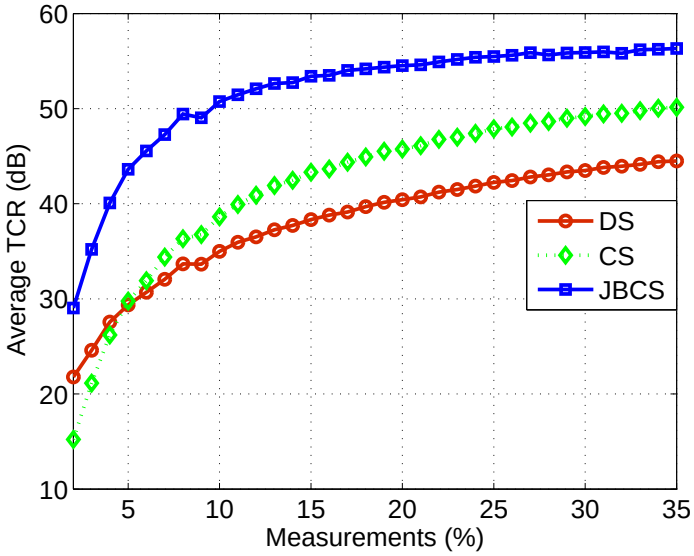


Figure 9. Comparison of the performance between the conventional DS beamforming, CS and the proposed JBCS approaches in terms of the average TCR of the formed images.

## Acknowledgments

We thank the Center of Advanced Communications at Villanova University, USA for providing the real TWRI data used in the experiments. This work was supported in part by a grant from the *Australian Research Council*.

## REFERENCES


[1] Ahmad, F., Amin, M. G., and Kassam, S. A., "Synthetic aperture beamformer for imaging through a dielectric wall," *IEEE Trans. Aerospace and Electronic Systems* **41**(1), 271–283 (2005).

[2] Amin, M. G. and Ahmad, F., "Wideband synthetic aperture beamforming for through-the-wall imaging," *IEEE Signal Processing Magazine* **25**(4), 110–113 (2008).

[3] Genyuan, W. and Amin, M. G., "Imaging through unknown walls using different standoff distances," *IEEE Trans. Signal Processing* **54**(10), 4015–4025 (2006).

[4] Seng, C. H., Bouzerdoum, A., Amin, M. G., and Phung, S. L., "Two-stage fuzzy fusion with applications to through-the-wall radar imaging," *IEEE Geoscience and Remote Sensing Letters* **10**(4), 687–691 (2012).

[5] Donoho, D. L., "Compressed sensing," *IEEE Trans. Information Theory* **52**(4), 1289–1306 (2006).

[6] Candes, E. J., Romberg, J., and Tao, T., "Stable signal recovery from incomplete and inaccurate measurements," *Communications on Pure and Applied Mathematics* **59**(8), 1207– 1223 (2006).

[7] Yoon, Y.-S. and Amin, M. G., "Compressed sensing technique for high-resolution radar imaging," in [*Proc. SPIE: Signal Processing, Sensor Fusion, and Target Recognition XVII*], **6968**, 69681A–69681A–10 (2008).

[8] Huang, Q., Qu, L., Wu, B., and Fang, G., "UWB through-wall imaging based on compressive sensing," *IEEE Trans. Geoscience and Remote Sensing* **48**(3), 1408–1415 (2010).

[9] Yang, J., Bouzerdoum, A., Tivive, F. H. C., and Amin, M. G., "Multiple-measurement vector model and its application to through-the-wall radar imaging," in [*Proc. IEEE Int. Conf. Acoustics, Speech and Signal Processing*], 2672–2675 (2011).

[10] Yoon, Y.-S. and Amin, M. G., "Imaging of behind the wall targets using wideband beamforming with compressive sensing," in [*Proc. IEEE/SP Workshop on Statistical Signal Processing*], 93–96 (2009).

[11] Yoon, Y.-S. and Amin, M. G., "Through-the-wall radar imaging using compressive sensing along temporal frequency domain," in [*Proc. IEEE Int. Conf. Acoustics, Speech, and Signal Processing*], 2806–2809 (2010).

[12] Tang, V. H., Bouzerdoum, A., and Phung, S. L., "Two-stage through-the-wall radar image formation using compressive sensing," *Journal of Electronic Imaging* **22**(2), 021006–021006 (2013).

[13] Shihao, J., Ya, X., and Carin, L., "Bayesian compressive sensing," *IEEE Trans. Signal Processing* **56**(6), 2346–2356 (2008).

[14] Ji, S., Dunson, D., and Carin, L., "Multitask compressive sensing," *IEEE Trans. Signal Processing* **57**(1), 92–106 (2009).

[15] Tropp, J. A., Gilbert, A. C., and Strauss, M. J., "Algorithms for simultaneous sparse approximation. part I: Greedy pursuit," *Signal Processing* **86**(3), 572–588 (2006).

[16] Cotter, S. F., Rao, B. D., Kjersti, E., and Kreutz-Delgado, K., "Sparse solutions to linear inverse problems with multiple measurement vectors," *IEEE Trans. Signal Processing* **53**(7), 2477–2488 (2005).

[17] Tropp, J. A., "Algorithms for simultaneous sparse approximation. part II: Convex relaxation," *Signal Processing* **86**(3), 589–602 (2006).

[18] Ahmad, F. and Amin, M. G., "Partially sparse reconstruction of behind-the-wall scenes," *Proc. SPIE* **8365-33** (2012).

[19] Amin, M. G., Ahmad, F., and Wenji, Z., "Target RCS exploitations in compressive sensing for through wall imaging," in [*Proc. Int. Waveform Diversity and Design Conf.*], 150–154 (2010).

[20] Tipping, M. E., "Sparse Bayesian learning and the relevance vector machine," *Journal of Machine Learning Research* **1**, 211–244 (2001).

[21] Chen, S. S., Donoho, D. L., and Saunders, M. A., "Atomic decomposition by basis pursuit," *SIAM Journal on Scientific Computing* **20**, 33–61 (1999).

[22] Gurbuz, A. C., McClellan, J. H., and Scott, W. R., "A compressive sensing data acquisition and imaging method for stepped frequency GPRs," *IEEE Trans. Signal Processing* **57**(7), 2640–2650 (2009).